Progress In Electromagnetics Research M, Vol. 107, 231–242, 2022

An Analytic Model for Stripline/Microstrip Potential Using Infinite Series with Mixed Boundary Conditions

James R. Nagel*

Abstract—This paper derives an infinite series solution to the Laplace equation for the electric scalar potential of a stripline/microstrip transmission line. Due to the presence of a mixed Dirichlet/Neumann boundary condition, traditional solution methods involving mode orthogonality cannot be applied. Instead, three new solution methods are explored, which are collocation, minimum discrete-squared error (MDSE), and minimum mean-squared error (MMSE). Results yield excellent agreement compared to numerical simulation of capacitance per unit length. However, the Gibbs phenomenon appears to bias the outcome with a small ($\approx 0.5\%$) under-estimation of the true result.

1. INTRODUCTION

One of the most widely utilized embodiments within the field of microwave engineering is stripline/microstrip transmission line [1, 2]. The structure is inexpensive to produce and has very high precision, and it is readily integrated into high-speed electronic circuits [3]. This makes the stripline a highly versatile tool, and full chapters are devoted to the subject in many standard textbooks.

Despite its popularity, the basic geometry has proved difficult to model using closed-form mathematical expressions. One method that has historically found use is conformal mapping [6–9], but the technique is not easily accessible to those with a typical mathematical background in engineering. It is also a mixed analytic-numerical method that requires both numerical integration and matrix inversion to calculate a solution. Alternatively, one could apply a crude approximation to the model by representing the charge density along the stripline as constant [5]. Thus, by sacrificing a little accuracy, a tractable mathematical solution is gained. A third option is to synthesize a closed-form expression that merely approximates the exact solution over a limited set of parameters [2, 4, 5, 10]. However, the result does not provide a complete physical account of the electric field profile. Finally, there is always the option of numerical simulation via the finite-difference/finite-element method or the boundary-element method [11–13], but these are brute-force approaches that often require expensive commercial software and specialized training in numerical methods.

In principle, there ought to exist an infinite series solution to the Laplace equation that models a stripline geometry under appropriate boundary conditions. Usually, such a procedure would apply an orthogonality relation to calculate the series coefficients [14]. For the special case of a stripline, however, the existence of a mixed Dirichlet/Neumann boundary condition makes this impossible. Historically, it seems that this type of problem has been neglected in the literature, but recent publications have begun to introduce new techniques. Most notably, W. W. Read discussed a number of methods in 2007 [15], thus giving us the mathematical tools to finally calculate a series solution.

In this paper, the author will apply three techniques to the classic stripline geometry: collocation, minimum discrete squared error (MDSE), and minimum mean-squared error (MMSE). In theory, each technique is exact, provided that the series solution is allowed to contain an infinite number of terms. Thus, the only approximation is a result of truncation to a finite series. If the stripline boundaries are

Received 16 August 2021, Accepted 31 January 2022, Scheduled 1 February 2022
* Corresponding author: James R. Nagel (james.nagel@utah.edu).
The author is with the Department of Electrical and Computer Engineering, University of Utah, Salt Lake City, UT 84112, USA.

allowed to approach infinity, then the geometry also converges to that of a microstrip. In this case, there is also the added approximation due to finite truncation of the domain itself.

The practical advantages of this new mathematical approach are numerous. First, most upper-division students of electrical engineering are already familiar with the basic formalism for solving the Laplace equation under specified boundary conditions, and the application to a mixed condition is only a small extension of this training. Furthermore, not all organizations have access to (or training in) expensive simulation software, and so a series solution can be invaluable for designers with limited resources (e.g., undergraduate students in microwave engineering). Computational speed is another advantage, in that a series solution will almost always be much faster (and more accurate) to process than a densely sampled simulation. Finally, the techniques presented in this paper can, in principle, be applied to a much wider class of engineering problems. For example, the coupled stripline is common embodiment encountered in high-speed digital communication [16, 17], and the geometry is very similar to that of a single stripline in isolation.

2. GENERAL SOLUTION

Figure 1 shows the standard layout for a stripline geometry. A thin, conductive strip with width W lies centered at the origin and is excited to an electric scalar potential of ϕ_0 volts. The strip is then enclosed in a perfectly conductive box that is grounded to a scalar potential of 0.0 V. The box has a width $a > W$, and it is divided into two vertical regions. The top region has a height h_1 and is filled with some dielectric material given by $\epsilon_r = \epsilon_1$. Likewise, the bottom region has a height h_2 and is filled with its own dielectric material such that $\epsilon_r = \epsilon_2$.

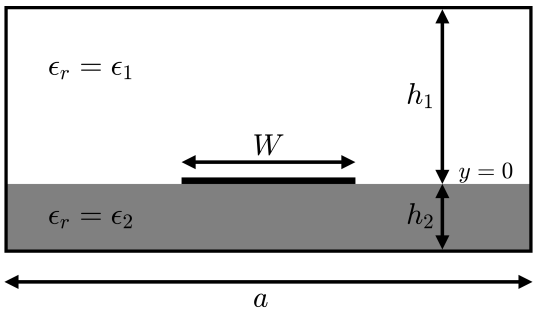

Figure 1. Cross-sectional view of the basic stripline geometry. The center conductive strip lies at the origin $(0, 0)$ and is excited to a potential of ϕ_0. The substrate has a thickness of h_2 with a ceiling height of h_1. The side walls are then grounded to a potential of $\phi = 0$.

Although any real stripline conductor must have finite thickness, typical real-world values are usually so small as to be regarded as zero. It is also common to consider the special case where $a \to \infty$ and $h_1 \to \infty$. In this case, the stripline geometry converges to that of a microstrip. Thus, any mathematical solution to the stripline can also be used to model a microstrip, provided that a and h_1 are allowed to grow very large.

The governing equation for any source-free electrostatic system is the Laplace equation,

$$\nabla^2 \phi = 0, \tag{1}$$

where ϕ is the electric scalar potential. For the stripline, we assume a general solution of

$$\phi(x, y) = [A\cos(kx) + B\sin(kx)]\left[Ce^{-ky} + De^{+ky}\right]. \tag{2}$$

Since the geometry of our system has even symmetry about $x = 0$, we may drop the sine-dependence and consider only the region defined by $x \in [0, a/2]$. It is also necessary to divide the solution into an upper ($y \geq 0$) and a lower ($y \leq 0$) region with solutions ϕ_1 and ϕ_2, respectively. This implies two general solutions with the form

$$\phi_1(x, y) = A\cos(kx)\left(e^{-ky} - Be^{+ky}\right) \quad [y \geq 0], \tag{3}$$

and

$$\phi_2(x,y) = C\cos(kx)\left(e^{+ky} - De^{-ky}\right) \quad [y \le 0]. \tag{4}$$

Letting each function equal zero beyond its respective region, we may write the total solution as simply $\phi = \phi_1 + \phi_2$.

We are now ready to impose our first boundary condition, which simply requires that

$$\phi(a,y) = 0. \tag{5}$$

This immediately forces us to conclude that the separation constant k satisfies an infinite set of possible values, written as

$$k_n = \frac{(2n-1)\pi}{a}, \quad n = 1,\, 2,\, 3\,\ldots \tag{6}$$

Since each of these values represents a potential solution, any linear combination of solutions must also be a solution. Our two potential functions therefore transform into infinite series with the form

$$\phi_1 = \sum_{n=1}^{\infty} A_n \cos(k_n x)\left(e^{-k_n y} - B_n e^{+k_n y}\right), \tag{7}$$

and

$$\phi_2 = \sum_{n=1}^{\infty} C_n \cos(k_n x)\left(e^{+k_n y} - D_n e^{-k_n y}\right). \tag{8}$$

Next, we require the potential at the top and bottom boundaries to be zero, giving us

$$\phi_1(x,+h_1) = 0, \quad \text{and} \tag{9}$$

$$\phi_2(x,-h_2) = 0. \tag{10}$$

This condition rapidly forces us to conclude that

$$B_n = e^{-2k_n h_1}, \quad \text{and} \tag{11}$$

$$D_n = e^{-2k_n h_2}. \tag{12}$$

We also require that the potential be continuous across the boundary at $y = 0$:

$$\phi_1(x,0) = \phi_2(x,0). \tag{13}$$

This condition implies the relationship

$$A_n(1 - B_n) = C_n(1 - D_n). \tag{14}$$

We next define the ratio

$$\alpha_n = \frac{1 - B_n}{1 - D_n} \tag{15}$$

so that $C_n = \alpha_n A_n$.

3. ELECTRIC FIELD PROFILE

Once a solution has been obtained for ϕ, we may now calculate the electric field profile given by $\mathbf{E} = -\nabla\phi$. Starting with the top region ($y > 0$), the x- and y-components satisfy

$$E_{x1} = \sum_{n=1}^{N} A_n k_n \sin(k_n x)\left(e^{-k_n y} - B_n e^{+k_n y}\right), \tag{16}$$

$$E_{y1} = \sum_{n=1}^{N} A_n k_n \cos(k_n x)\left(e^{-k_n y} + B_n e^{+k_n y}\right). \tag{17}$$

Likewise, the bottom region ($y < 0$) yields

$$E_{x2} = +\sum_{n=1}^{N} C_n k_n \sin(k_n x)\left(e^{+k_n y} - D_n e^{-k_n y}\right), \tag{18}$$

$$E_{y2} = -\sum_{n=1}^{N} C_n k_n \cos(k_n x)\left(e^{+k_n y} + D_n e^{-k_n y}\right). \tag{19}$$

4. MIXED BOUNDARY CONDITIONS

Clearly, the only remaining step is to calculate the series of Fourier coefficients represented by A_n. Ordinarily, this would involve one final boundary condition along the plane at $y = 0$, but the stripline geometry presents an unusual obstacle. Rather than impose a simple Dirichlet or Neumann boundary condition, we must instead impose a condition known as a *mixed boundary condition*. It means that the boundary at $y = 0$ is composed of a combination of Dirichlet and Neumann conditions simultaneously.

The first piece of our mixed boundary is a Dirichlet condition that imposes a constant scalar potential along the stripline, which we can write as

$$\phi(x, 0) = \phi_0 \quad (x \in [0, W/2]). \tag{20}$$

Substituting Eq. (7) therefore yields

$$\phi_0 = \sum_{n=1}^{\infty} A_n \cos(k_n x)\,(1 - B_n) \quad (x \in [0, W/2]). \tag{21}$$

Next, the Neumann boundary represents the standard condition for a dielectric interface, and it requires that

$$\epsilon_1 \frac{\partial \phi_1}{\partial y} = \epsilon_2 \frac{\partial \phi_2}{\partial y} \quad (x \in [W/2, a/2]). \tag{22}$$

Substituting Eqs. (17) and (19) thus yields the series equation

$$\sum_{n=1}^{\infty} A_n \gamma_n \cos(k_n x) = 0 \quad (x \in [W/2, a/2]), \tag{23}$$

where the γ_n coefficients are given by

$$\gamma_n = k_n \left[\epsilon_{r1}\,(1 + B_n) + \epsilon_{r2}\alpha_n\,(1 + D_n)\right]. \tag{24}$$

The difficulty with a mixed boundary condition is that it does not allow for the usual exploitation of orthogonality when calculating each A_n. As a result, there is no immediately obvious procedure towards a stable solution. Fortunately, recent publications have begun to provide a number of workable solutions [15], and the following sections will explore three of them with our present stripline problem.

5. COLLOCATION

One simple technique is called collocation, and it works by directly imposing the desired boundary condition along a discrete set of N arbitrary points [18]. The series defined by ϕ_1 and ϕ_2 are then truncated to N places, yielding a system of N equations with N unknowns. Thus, for every sample satisfying $x_m \leq W/2$, we impose the condition

$$\phi_0 = \sum_{n=1}^{N} A_n \cos(k_n x_m)\,(1 - B_n)\,. \tag{25}$$

Likewise, for every sample $x_m \in [W/2, a/2]$, we impose the dielectric boundary condition to find that

$$0 = \sum_{n=1}^{N} A_n \gamma_n \cos(k_n x_m). \tag{26}$$

Next, we define the column vector $\mathbf{a}$ to represent an array of unknown coefficients such that

$$\mathbf{a} = [A_1,\, A_2,\, A_3,\, \ldots,\, A_N]^T\,. \tag{27}$$

We further define the forcing vector $\mathbf{b}$ such that

$$b_m = \begin{cases} \phi_0 & x_m \in [0, W/2] \\ 0 & x_m \in [W/2, a/2] \end{cases} \tag{28}$$

We now have a matrix-vector equation with the form

$$\mathbf{Ua} = \mathbf{b}, \tag{29}$$

where the system matrix $\mathbf{U}$ is an $N \times N$ matrix satisfying

$$U_{mn} = \begin{cases} (1 - B_n)\cos(k_n x_m) & x_m \in [0, W/2] \\ \gamma_n \cos(k_n x_m) & x_m \in [W/2, a/2] \end{cases} \tag{30}$$

The solution is thus the simple inversion $\mathbf{a} = \mathbf{U}^{-1}\mathbf{b}$.

6. MINIMUM DISCRETE-SQUARED ERROR (MDSE)

Another simple solution method expands on the collocation principle by sampling an arbitrary set of M locations where $M > N$. Rather than force the boundary to be satisfied at all locations, however, we add up the total squared error and then minimize it. The procedure begins by introducing the error functions, $\mathcal{E}_1$ and $\mathcal{E}_2$, which represent the error between the truncated series expansion and the desired boundary condition. Starting with the Dirichlet condition, we have

$$\mathcal{E}_1(x_m) = -\phi_0 + w_1 \sum_{n=1}^{N} A_n \cos(k_n x_m)\,(1 - B_n)\,. \tag{31}$$

For the Neumann condition, we then let

$$\mathcal{E}_2(x_m) = w_2 \sum_{n=1}^{N} A_n \gamma_n \cos(k_n x_m). \tag{32}$$

The weighting coefficients (w_1, w_2) are important, as they scale the relative significance of each error. We can also think of them as constants of proportionality that equalize the units, given that $\mathcal{E}_1$ has units of volts, and $\mathcal{E}_2$ has units of volts per meter. Strictly speaking, however, we are only interested in the relative weight between the errors, since the absolute magnitude will be minimized either way. We may therefore assume $w_1 = 1$ and let w_2 serve as the only variable in this context.

Now consider a sampling of error across M different locations. This implies a vector $\mathbf{e}$ of M unique errors satisfying

$$\mathbf{e} = -\mathbf{b} + \mathbf{Ua}, \tag{33}$$

where the system matrix $\mathbf{U}$ is now $M \times N$. We next calculate the total squared error using

$$\mathbf{e}^T\mathbf{e} = \mathbf{b}^T\mathbf{B} - 2\mathbf{b}^T\mathbf{Ua} + \mathbf{a}^T\mathbf{U}^T\mathbf{Ua}. \tag{34}$$

Finally, we minimize the error by taking the derivative with respect to the vector $\mathbf{a}$ and then setting it to zero. Solving for $\mathbf{a}$ then yields

$$\mathbf{a} = (\mathbf{U}^T\mathbf{U})^{-1}\mathbf{U}^T\mathbf{b}. \tag{35}$$

7. MINIMUM MEAN-SQUARED ERROR (MMSE)

Our third solution technique is a popular procedure used throughout electrical engineering and signal processing. Rather than evaluate the error at a discrete location in space, we can minimize the total mean-squared error across the entire boundary region. We begin by defining the mean-squared errors $\bar{\mathcal{E}}_1$ and $\bar{\mathcal{E}}_2$ such that

$$\bar{\mathcal{E}}_1 = \frac{2}{W} \int_0^{W/2} |\mathcal{E}_1(x)|^2 dx, \quad \text{and} \tag{36}$$

$$\bar{\mathcal{E}}_2 = \frac{2}{a - W} \int_{W/2}^{a/2} |\mathcal{E}_2(x)|^2 dx. \tag{37}$$

Next, we substitute Eq. (31) into (36) to find

$$\bar{\mathcal{E}}_1 = \phi_0^2 - 2\phi_0 \sum_{n=1}^{N} u_n A_n + \sum_{m=1}^{N}\sum_{n=1}^{N} A_m M_{mn} A_n, \tag{38}$$

where the coefficients u_n and M_{mn} satisfy

$$u_n = \frac{2}{W} \int_0^{W/2} \cos(k_n x) dx, \tag{39}$$

$$M_{mn} = \frac{2}{W} \int_0^{W/2} \cos(k_n x)\cos(k_m x) dx. \tag{40}$$

Using matrix-vector notation, we can express this in a compact form as

$$\bar{\mathcal{E}}_1 = \phi_0^2 - 2\phi_0 \mathbf{u}^T\mathbf{a} + \mathbf{x}^T\mathbf{M}\mathbf{a}. \tag{41}$$

Following a similar procedure, we express the second error term as

$$\bar{\mathcal{E}}_2 = \mathbf{a}^T\mathbf{N}\mathbf{a}, \tag{42}$$

where the matrix elements N_{mn} satisfy

$$N_{mn} = \frac{2\gamma_n\gamma_m}{a-W} \int_{W/2}^{a/2} \cos(k_n x)\cos(k_m x) dx. \tag{43}$$

For convenience, the solution to this integral is provided in Appendix A.

The last step is to combine our two errors and then minimize the sum. Begin by reintroducing the weight coefficients (w_1, w_2) to define the weighted sum as

$$\bar{\mathcal{E}} = w_1\bar{\mathcal{E}}_1 + w_2\bar{\mathcal{E}}_2. \tag{44}$$

As before, the absolute magnitude of the error is not important, but the relative error is. We therefore let $w_1 = 1$ and assume that w_2 is the only parameter allowed to vary. When being expressed in matrix-vector notation, this is evaluated to

$$\bar{\mathcal{E}} = \phi_0^2 - 2\phi_0 \mathbf{u}^T\mathbf{a} + \mathbf{a}^T\mathbf{M}\mathbf{a} + w_2\mathbf{x}^T\mathbf{N}\mathbf{a}. \tag{45}$$

Finally, we again differentiate with respect to the vector $\mathbf{a}$ and then set it to zero. The solution is

$$\mathbf{a} = (\mathbf{M} + w_2\mathbf{N})^{-1}(\phi_0\mathbf{u}). \tag{46}$$

8. DEMONSTRATION

As a demonstration case, Fig. 2 shows the calculation of electric scalar potential ϕ and electric field intensity $\mathbf{E}$ for a typical stripline/microstrip geometry. The model parameters are given as follows:

$$\begin{aligned}
\phi_0 &= 1.0\,\mathrm{V} \\
W &= 4.0\,\mathrm{mm} \\
a &= 15\,\mathrm{mm} \\
h_1 &= 1.25\,\mathrm{mm} \\
h_2 &= 6.30\,\mathrm{mm} \\
\epsilon_{r1} &= 1 \\
\epsilon_{r2} &= 4.4 \\
N &= 255
\end{aligned}$$

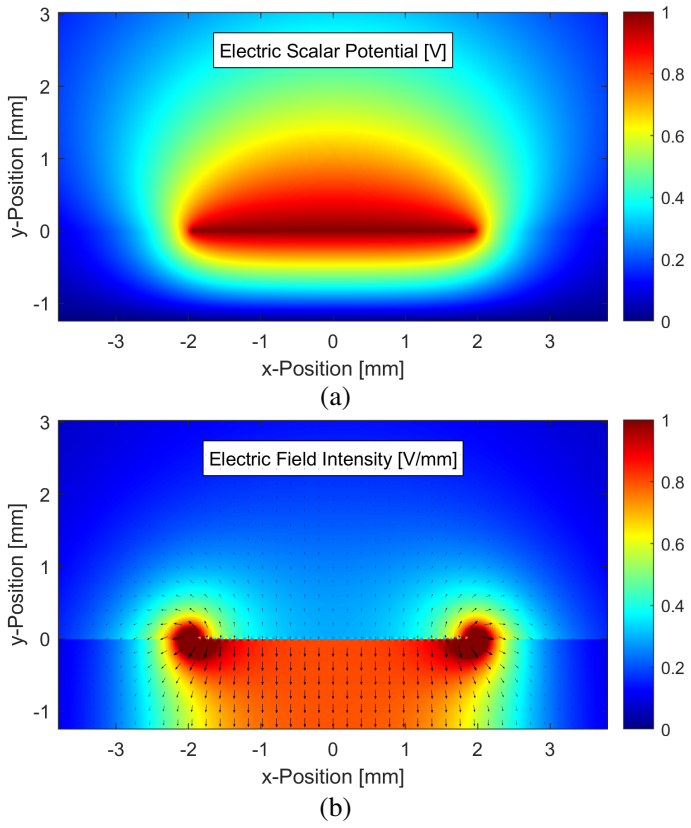

Figure 2. (a) Electric scalar potential of a stripline with width $W = 4.4\,\text{mm}$. The substrate has a height $h_2 = 1.25\,\text{mm}$ with a dielectric constant of $\epsilon_{r2} = 4.4$. (b) Corresponding electric field profile.

The solution was calculated using MMSE and required only 4.5 ms to calculate the expansion coefficients on a standard laptop computer.

The optimal choice of weight coefficients (w_1, w_2) is not immediately obvious, as there are many possible reasons for preferring some values over others. For example, a very large value of w_2 would bias the solution towards extremely high accuracy for the Neumann condition while sacrificing accuracy along the Dirichlet. In practice, however, it seems intuitive that the error in each region should at least be equalized in scale. One straightforward technique for achieving this goal is to normalize the error $\mathcal{E}_2$ by γ_1. For MMSE, this implies $w_2 = 1/\gamma_1^2$. For MDSE, we then have $w_2 = 1/\gamma_1$.

It is interesting to note the distinct ripples in the electric field profile around the stripline itself. This is a direct result of the Gibbs phenomenon, which is exacerbated whenever one attempts to fit a Fourier series to a non-smooth function. Fig. 3 explores this behavior in detail by examining ϕ and E_{y2} along the boundary at $y = 0$. Using collocation, the Gibbs phenomenon appears to be mitigated rather well along the stripline. Along the dielectric boundary, however, there appears to be significant oscillation in the electric field, even as N grows very large. MDSE and MMSE, however, appear to exhibit the opposite behavior. Fitting to the boundary along the strip is relatively weak, but the electric field profile is smoother along the dielectric boundary. It is also interesting to note how MDSE and MMSE appear to produce very similar results.

9. SURFACE CHARGE DENSITY AND CAPACITANCE

Another useful parameter we are interested in is the characteristic capacitance between the stripline and the ground plane. By definition, this is given as

$$C' = \frac{Q'}{\phi_0}, \tag{47}$$

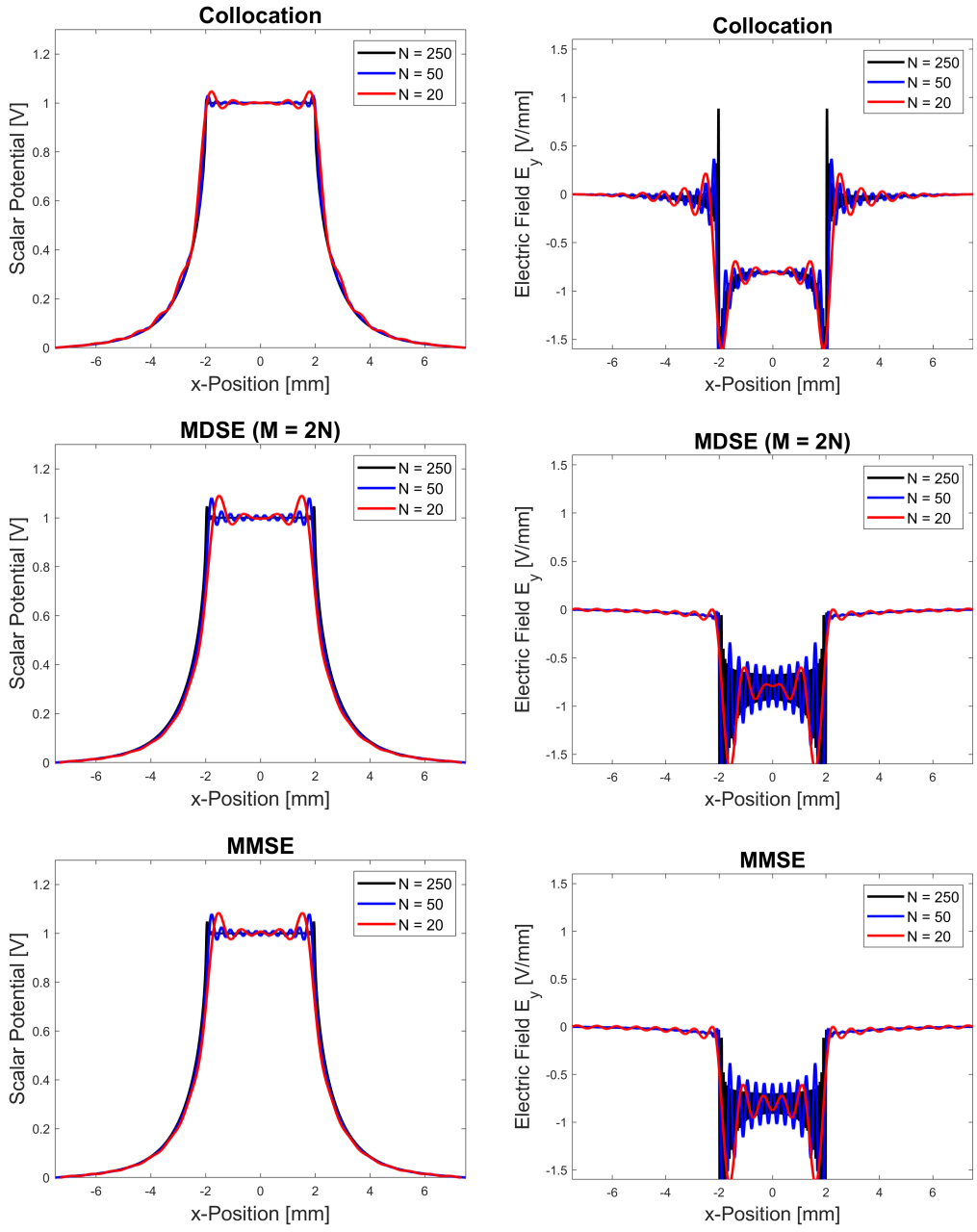

Figure 3. An exploration of the convergence behavior for each solution method along the boundary at $y = 0$. Plots of the left show the electric scalar potential $\phi(x, 0)$. Plots on the right depict $E_{y2}(x, 0)$.

where C' has units of F/m, and Q' is the linear charge density with units of C/m. Since the potential difference ϕ_0 is given, we only need to calculate Q'. Assuming a closed contour integral along the clockwise direction, Gauss' law dictates that

$$Q' = \oint \epsilon_0 \epsilon_r \mathbf{E} \cdot d\hat{\mathbf{n}}, \tag{48}$$

where $d\hat{\mathbf{n}}$ is the differential unit normal vector along the contour. Since the contour itself is arbitrary, we can imagine an infinitesimally thin rectangle that perfectly encloses the stripline. The contribution from the x-component of the electric field is thus negligible, leaving just the contribution from E_{y1} over the top of the strip and E_{y2} along the bottom. By exploiting symmetry about the origin, we can express

the resulting integral as

$$Q' = 2\epsilon_0 \int_0^{W/2} (\epsilon_{r1} E_{y1} - \epsilon_{r2} E_{y2}) dx. \tag{49}$$

If we then substitute the series expansions from Eqs. (17) and (19), the integral is evaluated to

$$Q' = 2\epsilon_0 \sum_{n=1}^{N} A_n (\gamma_n / k_n) \sin(k_n W/2). \tag{50}$$

We can also use this expression to calculate the surface charge density $\sigma(x)$ by imagining the differential contribution dQ' along the differential length dx. Letting $dQ'/dx = \sigma(x)$, we then find

$$\sigma(x) = \epsilon_0 \sum_{n=1}^{N} A_n \gamma_n \cos(k_n x). \tag{51}$$

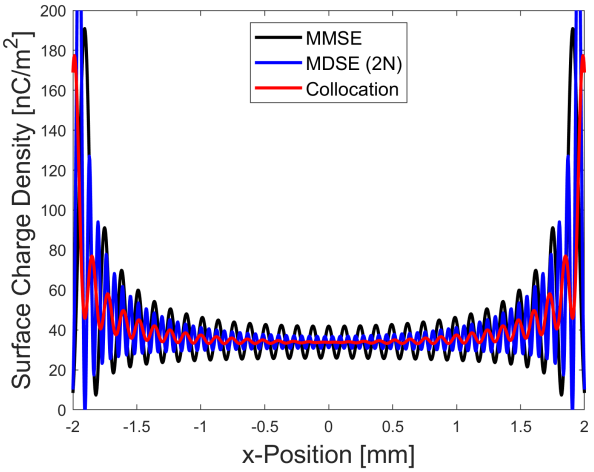

Figure 4. Surface charge density profile $\sigma(x)$ along the stripline using $N = 100$ modes.

Figure 4 shows a calculation of $\sigma(x)$ for a stripline under the same geometry as that in Fig. 2, but with $N = 100$. As expected, the surface charge density diverges near the edge of the stripline, which is consistent with the electrostatic behavior of a charged surface. This makes it intrinsically difficult to capture the behavior of the surface charge profile using a Fourier series, and so we may expect some inherent error when calculating C'. To quantify this error, the same stripline geometry was numerically simulated using the finite-difference method [11] under a grid spacing of $\Delta x = 12.6\,\mu$m. The characteristic capacitance was then calculated as a function of mode number N using each of the three solution methods. The results of that comparison are summarized in Fig. 5.

The first interesting observation is that collocation tends to be highly unstable for this sort of calculation. The cause appears to be the uniform grid sampling that was used to match the boundary conditions. As a result, the grid sampling near $x = W/2$ tends to haphazardly catch or miss the singularity around the edge, depending on the value of N. In the future, this can potentially be remedied by enforcing a non-uniform grid sampling that always includes $x = W/2$. However, one must be careful with this sort of procedure, as non-uniform sampling can potentially destabilize the solution. For MDSE, we likewise observe a similar jitter, but it appears greatly reduced as a result of the over-sampling with $M = 2N$. MMSE appears to be most stable of all, which is expected from the averaging across each interval.

It is interesting to note that all three methods appear to consistently under-calculate the true capacitance. Even at the comparatively large value of $N = 1000$, the calculation error is still about -0.25%. Part of this is almost certainly due to numerical error with simulation itself, but we also

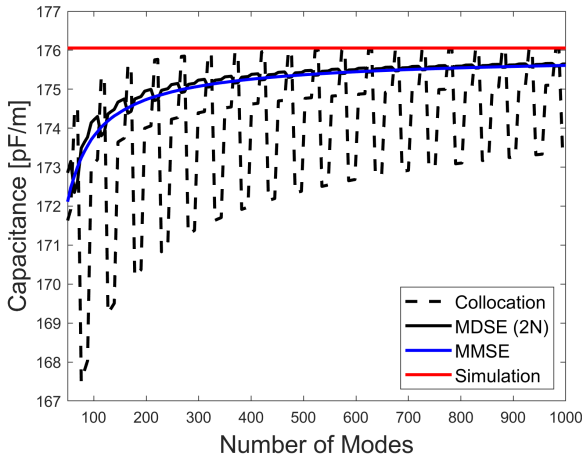

Figure 5. Convergence of the characteristic capacitance C' as a function of total modes N.

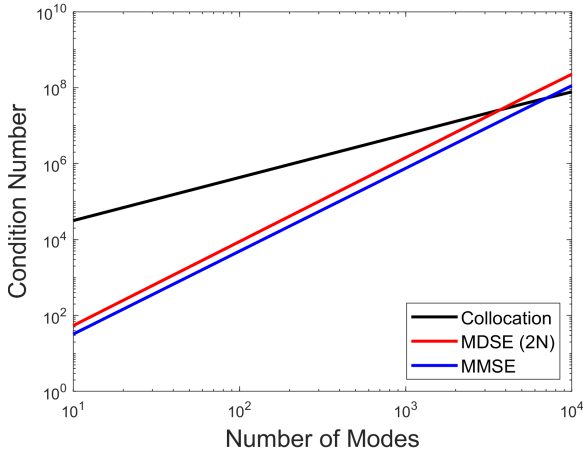

Figure 6. System matrix condition number as a function of total modes N.

know that the Fourier series struggles with the singular behavior of $\sigma(x)$ near the edge of the stripline. In principle, this error ought to shrink to zero as $N \to \infty$, but the computational effort required to express that final piece of the model seems prohibitive. In practice, however, the error seems well within tolerance for most applications, but it would still be worth the effort to explore any methods that alleviate this final bit of uncertainty.

10. NUMERICAL STABILITY

In principle, the mathematical error of any series solution should reduce to zero as the number of terms is increased to infinity. In practice, however, the use of matrix inversion has the potential to destabilize the solution if conditioning is very poor. It is therefore important to quantify the numerical stability of each solution method as the number of terms grows very large.

Figure 6 explores this relationship by calculating the condition number for the system matrix $\mathbf{U}$ as the total number of coefficients is increased. For the special case of MDSE, the condition number is calculated for $\mathbf{U}^T\mathbf{U}$ since this is the matrix that ultimately gets inverted. Immediately, we see that collocation is the least stable of all three methods, but that MDSE and MMSE eventually overtake it for very large N. The most useful finding is that, even at the comparatively large value of $N = 10000$, the condition number is only on the scale of about 10^8. For noise-free double-precision arithmetic, this is a very reasonable value, and instability will generally not manifest until the condition number reaches upwards of 10^{15}.

11. DISCUSSION

This paper shows how to model the classic stripline geometry as an infinite series solution to the Laplace equation. The key obstacle was a mixed boundary condition along $y = 0$, which cannot be solved using traditional orthogonality relations. Instead, the solution was expressed in terms of error minimization along each respective boundary condition. This introduces a number of interesting avenues of research, in that many other useful configurations can potentially be solved using similar methods. For example, the coupled stripline is a common embodiment with many practical applications [16, 17, 19], and it seems straightforward to construct a corresponding model using the same mathematical techniques. For the even-mode symmetric stripline, we would simply add a Neumann boundary condition at the center and then impose a second mixed boundary condition for the space between lines. For the odd-mode case, we would then repeat the analysis with a Dirichlet boundary condition at the center.

As noted earlier, the key distinction between a stripline and a microstrip is the size of the domain enclosing the central strip. Thus, in order to model a true microstrip, we need to let $h_1 \to \infty$ and

$a \to \infty$. The first condition is numerically stable, as it merely forces $B_n = 0$. The second condition, however, cannot be realized with a finite value for N. Thus, the trick is to allow a to grow reasonably large, but not so large that the N becomes prohibitively large as well. We must also be careful not to destabilize the solution, as it is unclear how well conditioned the system matrix will remain under such stress.

Finally, the singular behavior of charge density around the edges of the stripline poses an interesting mathematical challenge. Since the Fourier series cannot perfectly capture the sharp edge in scalar potential, the model tends to behave as if the stripline is slightly shorter than it truly is. In practice, this small amount of error may be tolerable, but it is unclear whether or not it will remain so under all possible conditions. This is a question that may require further investigation if the same technique is applied to more complex geometries.

APPENDIX A.

We are interested in evaluating the integral with the following form:

$$I = \int_a^b \cos(k_n x)\cos(k_m x)dx. \tag{A1}$$

Using the product identity, we can rewrite the integrand as

$$\cos(k_n x)\cos(k_m x) = \frac{\cos(ux) + \cos(vx)}{2}, \tag{A2}$$

where $u = k_n - k_m$ and $v = k_n + k_m$. For the special case of $k_n = k_m = k$, we find that

$$I = \frac{b-a}{2} + \frac{\sin(2kb) - \sin(2ka)}{4k}. \tag{A3}$$

For $k_n \neq k_m$, we have

$$I = \frac{\sin(ub) - \sin(ua)}{2u} + \frac{\sin(vb) - \sin(va)}{2v}. \tag{A4}$$

REFERENCES

1. Maloratsky, L. G., "Reviewing the basics of microstrip lines," *Microwaves & RF*, No. 3, 79–88, 2000.
2. Edwards, T. C. and M. B. Steer, *Foundations for Microstrip Circuit Design*, 4th Edition, Wiley-IEEE Press, 2016.
3. Khater, M. A., "High-speed printed circuit boards: A tutorial," *IEEE Circuits and Systems Magazine*, Vol. 20, No. 3, 34–45, 2020.
4. Ulaby, F. T. and U. Ravaioli, *Fundamentals of Applied Electromagnetics*, 7th Edition, Prentice Hall, Essex, 2015.
5. Pozar, D. M., *Microwave Engineering*, 4th Edition, Wiley, Hoboken, NJ, 2011.
6. Cohn, S. B., "Characteristic impedance of the shielded-strip transmission line," *Transactions of the IRE Professional Group on Microwave Theory and Techniques*, Vol. 2, No. 2, 52–57, 1977.
7. Rao, J. S. and B. N. Das, "Analysis of asymmetric stripline by conformal mapping," *IEEE Transactions on Microwave Theory and Techniques*, Vol. 27, No. 4, 299–303, 1979.
8. Homentcovschi, D., A. Maolescu, A. M. Manolescu, and L. Kreindler, "An analytical solution for the coupled stripline-like microstrip line problem," *IEEE Antennas and Propagation Magazine*, Vol. 36, No. 6, 1002–1007, 1988.
9. Cattaneo, P. W., "Capacitances in micro-strip detectors: A conformal mapping approach," *Solid-State Electronics*, Vol. 54, No. 1, 252–258, 2010.
10. Bahl, I. J. and D. K. Trivedi, "A designer's guide to microstrip line," *Microwaves*, Vol. 16, No. 5, 174–182, 1977.

11. Nagel, J. R., "Numerical solutions to Poisson equations using the finite difference method," *IEEE Antennas and Propagation Magazine*, Vol. 56, No. 4, 209–224, 2014.
12. Chang, T.-N. and C.-H. Tan, "Analysis of a shielded microstrip line with finite metallization thickness by the boundary element method," *IEEE Transactions on Microwave Theory and Techniques*, Vol. 38, No. 8, 1130–1132, 1990.
13. Peric, M., A. N. V. Sasa, S. Ilic, and N. B. Raicevic, "Improving the efficiency of hybrid boundary element method for electrostatic problems solving," *ACES Journal*, Vol. 35, No. 8, 872–877, 2020.
14. Powers, D. L., *Bounadry Value Problems and Partial Differential Equations*, 6th Edition, Elsevier, Burlington, 2010.
15. Read, W. W., "An analytic series method for laplacian problems with mixed boundary conditions," *Mathematics and Statistics*, Vol. 209, No. 1, 22–32, 2007.
16. Bryant, T. G. and J. A. Weiss, "Parameters of microstrip transmission lines and of coupled pairs of microstrip lines," *IEEE Transactions on Microwave Theory and Techniques*, Vol. 16, No. 12, 1021–1027, 1968.
17. Bahl, I. J. and P. Bhartia, "The design of broadside coupled stripline circuits," *IEEE Transactions on Microwave Theory and Techniques*, Vol. 29, No. 2, 165–168, 1981.
18. Trefethen, L. N., *Spectral Methods in MATLAB*, SIAM, Philadelphia, 2001.
19. Maloratsky, L. G., "Reviewing the basics of suspended striplines," *Microwave Journal*, 82–98, October 2002.